ARTICLE

Journal of Materials Chemistry
www.rsc.org/materials

A novel synthesis of nanocapsules using identical polymer core/shell nanospheres

Jyongsik Jang,* Joon Hak Oh and Xiang Li Li

Hyperstructured Organic Materials Research Center and School of Chemical Engineering, Seoul National University, Shinlimdong 56-1, Seoul 151-742, Korea. E-mail: jsjang@plaza.snu.ac.kr; Fax: +82 2 888 1604; Tel: +82 2 880 7069

Received 15th April 2004, Accepted 9th June 2004
First published as an Advance Article on the web 5th August 2004

Polymer nanocapsules were synthesized using core/shell nanospheres composed of an identical polymer. Linear polypyrrole (PPy)/crosslinked PPy core/shell nanospheres were synthesized stepwise by microemulsion polymerization using two oxidants with different chemical oxidation potentials, *i.e.* copper(II) chloride and iron(III) chloride. Coupled with the characteristics of the O/W microemulsion polymerization, the hydrophilic oxidants with different chemical oxidation potentials produced PPys with different solubility in alcohol. The linear PPy core and cationic surfactants could be removed by one-step solvent etching process simultaneously, and crosslinked PPy nanocapsules were obtained. The pore size and shell thickness of PPy nanocapsules were tunable by controlling the feeding amount of monomers in each synthetic step. The pore size of PPy nanocapsules was controllable from 19 to 33 nm by changing the monomer amount from 5.4 to 20.2 mmol in the first synthetic step. The shell thickness also increased gradually from 5.0 to 12.5 nm with increasing the feeding amount of monomers from 14.9 to 48.5 mmol in the second synthetic step. The average diameter of polymer nanocapsules could also be controllable by changing the surfactant concentration and surfactant spacer length. PPy nanocapsules had two mesopores, that is, the inner cavity and the mesochannel in the wall. In addition, PPy hollow nanospheres could be transformed into carbon nanocapsules through the carbonization process. The structural development of graphene layers in the carbon nanocapsule wall was investigated using XRD measurement, Raman spectroscopy, and HRTEM analysis. The ability to selectively encapsulate and release guest molecules was examined by introducing a photochromic dye (pyrene) solution into the polymer and carbon nanocapsules in a different environment.

Introduction

Over the last decade, there has been intense interest in the development of micro- and nano-sized capsules that consist of either organic or inorganic materials. Owing to their structural characteristics such as controllable permeability into the inner cavity, low density and large specific area, micro- and nano-sized capsules could find a wide range of potential applications including drug delivery,[1,2] nanostructured functional composites,[3–5] heterogeneous catalysis,[6,7] encapsulation of dye or pigment,[8,9] contaminated waste removal,[10] and protection of enzymes and proteins.[11,12]

Among the target materials, polymeric nanocapsules are of particular interest because of their ability to encapsulate a variety of guest molecules and modify the surface functionalities of host or guest molecules. In addition, the nano-sized dimension provides a facilitated permeation and absorption into biological tissues as well as an enhanced surface area. The growing demand for polymeric nanocapsules has expedited the development of various fabrication methods including colloidal templating,[13,14] layer-by-layer adsorption,[15,16] encapsulation of a non-solvent,[17,18] phase separation of block copolymers,[19,20] crosslinking of micellar coronas,[21,22] vesicles,[23] dendrimers,[24,25] and self-assembling approaches utilizing covalent bonds and hydrogen bonds.[26,27] However, most synthetic approaches have employed different materials as core and shell parts, for example, inorganic–organic, metallic–organic, and disparate organic–organic materials. The methods have also required multi-step etching processes to remove the core and the stabilizing agent.

In a previous communication,[28] we described a novel fabrication of polymer hollow nanospheres using core/shell nanomaterials composed of an identical polymer, for the first time. PPys with different solubility in alcohol were synthesized stepwise to form core/shell nanospheres by microemulsion polymerization using two kinds of oxidants. PPy nanocapsules were obtained by one-step solvent etching of the soluble core and the surfactant micelles. Carbon nanocapsules were fabricated by the carbonization of the polymeric nanocapsules.

In this paper, we demonstrate the structural characteristics of the polymer and carbon nanocapsules. The polymerization mechanism has been described with the structural formula. In addition, the nanocapsules were employed as a host container for the encapsulation of a photochromic dye molecule. The selective encapsulation/release behaviors of photochromic dye into the polymeric nanocapsules were observed in different environments, *i.e.* aqueous and organic media. The graphitization of carbon nanocapsule wall was also investigated by changing the carbonization temperatures.

Experimental

Materials

Pyrrole (98%) monomer was purchased from Aldrich and used as received. Copper(II) chloride (98%) and iron(III) chloride (97%), which were employed as the oxidants for the polymerization of pyrrole, were also obtained from Aldrich and used without further purification. 2,2,4-trimethylpentane (99%) was delivered from Aldrich and used as a nonsolvent for the precipitation of polymer nanoparticles. Pyrene (98%), which was used as a photochromic dye, was purchased from Aldrich and used as received. Cationic surfactants were employed to form microemulsion micelles as nanoreactors. Octyltrimethylammonium bromide (OTAB, 98%), decyltrimethylammonium bromide (DeTAB, 98%), and

DOI: 10.1039/b405607h

cetyltrimethylammonium bromide (CTAB, 98%) were obtained from Fluka and used without further purification. Tetrahydrofuran (THF, spectrophotometric grade) and benzene (spectrophotometric grade) were purchased from DC Chemical Co. and used as the organic medium of photochromic dye. Methyl alcohol (extra pure grade) was also purchased from DC Chemical Co and utilized as the etching solvent of linear PPy core and cationic surfactants.

Synthesis of PPy hollow nanospheres

A variable amount of surfactant, which ranged in the concentration between the critical micelle concentration (c.m.c.) I and c.m.c. II, was magnetically stirred in 40 mL of distilled water at 25 °C. To synthesize size-tunable linear PPy nanospheres as the core template, a different amount of pyrrole (5.4–20.2 mmol) was added dropwise to the micellar solution. After feeding pyrrole monomers completely, the micellar solution containing pyrrole monomers was magnetically stirred for 30 min. Then, copper(II) chloride (based on the half of the molar quantity of pyrrole) was dissolved in 5 mL of distilled water and the oxidant solution was added to the reaction mixture. The chemical oxidation polymerization of linear PPy core proceeded with magnetic stirring for 3 h at 25 °C.

To retrieve linear PPy nanoparticles, the reaction product was moved to a separation funnel and excess amount (over twentyfold of the reaction solution) of distilled water was poured into the separation funnel. As the surfactant molecules were dissolved into the aqueous solution, where the surfactant concentration became much lower than c.m.c. I, the synthesized PPy nanoparticles were precipitated. After the complete precipitation of PPy nanoparticles, the upper solution containing surfactants and residual oxidants was discarded and the PPy nanoparticle precipitate was dried in a vacuum oven at room temperature.

On the other hand, linear PPy/crosslinked PPy core/shell nanospheres could be fabricated through the consecutive synthesis of crosslinked PPy shell onto the linear PPy core, without the etching process described above. To synthesize crosslinked PPy shell with various wall thickness, a variable amount of pyrrole (14.9–48.5 mmol) was added dropwise to the reaction solution containing surfactant-coated linear PPy core. Iron(III) chloride (based on the half of the molar quantity of pyrrole) was dissolved in 5 mL of distilled water and the solution was added to the reaction mixture. The chemical oxidation polymerization of crosslinked PPy shell proceeded with magnetic stirring for 3 h at 25 °C.

After the chemical oxidation polymerization, the reaction product was moved to a separation funnel and excess amount (over twenty times the reaction solution) methyl alcohol was poured into the separation funnel. 2,2,4-trimethylpentane (50–100 mL) was added to promote the precipitation of the PPy nanocapsule. The facilitated precipitation of PPy nanocapsules was due to the enhanced hydrophobicity of the nonsolvent. After the precipitation of the reaction product, the upper solution containing surfactant, soluble PPy and unreacted oxidants was discarded and the PPy nanocapsule precipitate was dried in a vacuum oven at room temperature.

In a typical synthesis of PPy hollow nanospheres, 0.5 g (7.5 mmol) of pyrrole monomer was added dropwise to 0.45 M of DeTAB (40 mL), and 0.5 g (3.8 mmol) of copper(II) chloride was put into the surfactant/pyrrole solution. Chemical oxidation polymerization proceeded with magnetic stirring for 3 h at 25 °C. 1.0 g (14.9 mmol) of pyrrole monomer was added dropwise into the micellar solution. Iron(III) chloride (1.2 g, 7.4 mmol) was dissolved in a small amount of distilled water and the solution was added to the reaction mixture. After the chemical oxidation polymerization for 3 h at 25 °C, the reaction product was moved to a separation funnel and excess methyl alcohol was poured into the separation funnel. 2,2,4-trimethylpentane (50 mL) was added to promote the precipitation of the PPy nanocapsule. After the precipitation of the reaction product, the upper solution containing surfactant, soluble PPy and unreacted oxidants was discarded and the PPy nanocapsule precipitate was dried in a vacuum oven at room temperature.

Fabrication of carbon nanocapsules

A small amount of the crosslinked PPy nanocapsule was put into a quartz tube in an electric furnace under Ar flow (0.2 L min^{-1}). The sample was heated up to carbonization temperature (1000 °C or 1300 °C) at a heating rate 3 °C min^{-1}, held for 3 h, and then naturally cooled to room temperature.

Encapsulation and release of pyrene molecules

To examine the feasibility of controllable permeability of polymer and carbon nanocapsules, pyrene (1 mg) in THF (1 mL) was introduced into the mixture of nanocapsules (2 mg) in water (10 mL) and then vigorously stirred for 1 h. Benzene (10 mL) was also employed as a hydrophobic medium.

Instrumental analysis

Bright field (BF) transmission electron microscopy (TEM) images and energy-dispersive X-ray (EDX) data were taken using a JEOL EM-2000 EX II microscope and a Philips CM-20 microscope coupled with an EDX facility. High resolution (HR) TEM images were taken with a JEOL 2010 F microscope. The TEM observation was conducted at an acceleration voltage of 200 kV. Scanning electron microscopy (SEM) images were obtained with a JEOL JSM-6700 F microscope operated at an acceleration voltage of 5.0 kV. Elemental analysis was conducted with an EA 1110 apparatus (CE Instruments). Fourier-transform infrared (FT-IR) spectra were recorded on a Bomem MB 100 spectrometer using absorption mode. Thirty-two scans were collected with a spectral resolution of 4 cm^{-1}. X-ray diffraction (XRD) measurement was performed with a Rigaku DMAX-IIIA. Raman spectra were obtained using a Jobin-Yvon T64000 spectrometer equipped with an Ar-ion laser. Nitrogen adsorption isotherms were recorded with a Micromeritics ASAP 2000. Fluorescence images of pyrene-embedded capsules were taken with a Carl Zeiss LSM510 confocal laser scanning microscope (CLSM). The excitation wavelength was 488 nm and the scanning region was in the band path of 505–530 nm.

Results and discussion

Outline for the overall experimental procedures

Overall experimental procedure is illustrated in Scheme 1. Cationic surfactants such as OTAB, DeTAB, and CTAB were used to form micelles as nanoreactors. In an aqueous solution, cationic surfactants form micelles at the concentration over c.m.c. owing to the hydrophobic interactions of hydrocarbon spacers.[29–31] In those conditions, the strength of hydrophobic interactions exceeds that of electrostatic repulsions of ionic head groups, which stabilizes the formation of micelles. Hydrophobic alkyl chains remain tangled in a micelle.

In the synthetic procedure of PPy core/shell nanomaterials, pyrrole monomers and different oxidants, *i.e.* copper(II) chloride (E° = +0.16 V) and iron(III) chloride (E° = +0.77 V), were added stepwise into the micellar solution. Pyrrole monomers have poor solubility in water, whereas they are freely soluble in organic solvents such as benzene and ether. Therefore, pyrrole monomers are likely to be introduced into the hydrophobic inner space of a micelle, which causes the swelling of the micelle to some degree. Our previous results[32–35] also confirm that pyrrole monomers are incorporated into the

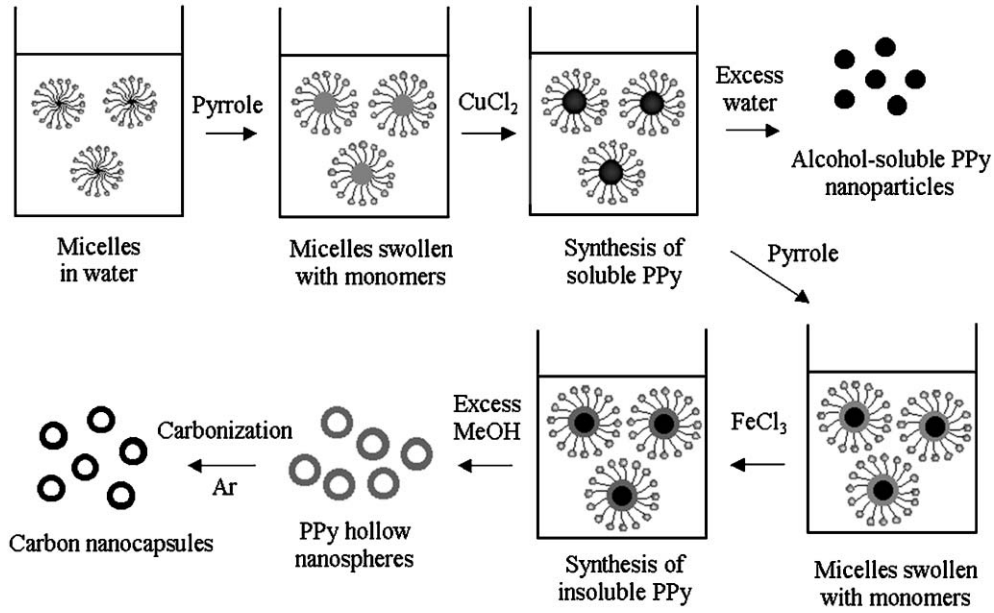

Scheme 1 Schematic representation of the fabrication of PPy and carbon hollow nanospheres.

inner space of a micelle in the microemulsion system. In theoretical aspect, it is also very difficult that hydrophobic monomer droplets exist separately in microemulsion system, due to the high concentration of surfactants (*i.e.* the large number of micelles).[36] In a control experiment where surfactants were not added, submicron-sized (100–200 nm diameter) particles with a broad particle size distribution were only synthesized.

Coupled with the characteristic of O/W microemulsion system, the hydrophilic oxidants with different chemical oxidation potentials produced PPys with different solubility in alcohol. Copper(II) chloride with lower oxidation potential produced linear PPy core, which was soluble in alcohol. On the other hand, iron(III) chloride with higher oxidation potential created crosslinked PPy shell, which was insoluble in alcohol. When excess methyl alcohol was added into the reaction solution, the linear PPy core was etched out along with the surfactants and the residual oxidants. The PPy nanocapsules were successfully utilized as precursors for carbon nanocapsules. The inner cavity size and shell thickness of hollow nanocapsules were tunable by controlling the concentration of surfactants and pyrrole monomers.

Synthesis of PPy nanocapsules

Fig. 1(a) represents a TEM image of soluble PPy nanoparticles synthesized by using pyrrole (7.5 mmol) and copper(II) chloride (3.8 mmol) in 0.45 M DeTAB. The number average diameters (D_n) of the soluble PPy templating core were measured directly from each TEM image and found to be approximately 23 nm. In the common procedure, the sizes of 50 particles were measured and the values were averaged. The D_n was calculated from following equation:[37]

$$D_n = \sum_i N_i D_i / \sum_i N_i$$

where D_i means the diameters of individual particles and N_i refers to the number of particles corresponding to the diameters.

The insoluble PPy shell was synthesized onto the surface of the soluble PPy core by adding pyrrole (14.9 mmol) and iron(III) chloride (7.4 mmol) subsequently. Judging from the SEM image (Fig. 1(b)), the linear PPy/crosslinked PPy core/shell nanomaterials consisted entirely of spherical particles with a mean diameter of 33 nm. The TEM image of the PPy core/shell nanospheres showed a slight difference in the contrast of the core and shell parts (the inset in Fig. 1(b)). Fig. 1(c) displays a TEM image of PPy nanocapsules prepared by etching the soluble PPy core with methyl alcohol. The average pore size of PPy hollow nanospheres was similar to the diameter of the soluble PPy core. This means that the soluble PPy core acted successfully as the template. The average wall thickness of PPy nanoparticles was about 5 nm.

The pore size distribution was calculated by the Barrett-Joyner-Halenda (BJH) method from the nitrogen adsorption isotherm branch at 350 K (Fig. 1(d)). The result revealed that the PPy nanocapsules contain two kinds of mesopores, *i.e.* about 2 nm and 23 nm. The large pore originates from the cavity size of polymer hollow nanospheres, which is consistent with the TEM image (Fig. 1(c)). The small pore is considered to be due to the mesochannels in the capsule wall that was seemingly generated during the solvent etching process.

The FT-IR spectrum of PPy nanocapsules is illustrated in Fig. 2. The FT-IR spectrum exhibited a slanted baseline presumably due to the plasma reflection phenomenon of the conducting polymer.[38] The broad peak at 3403 cm^{-1} was attributed to hydrogen bonded N–H stretching vibration and the small peaks at 2925 and 2851 cm^{-1} originated from five-membered ring C–H stretching vibration. The bands at 1547, 1485, and 784 cm^{-1} were due to free C–N stretching vibration, conjugated C–N stretching vibration, and C–H wagging vibration, respectively.

According to elemental analysis, PPy nanocapsules consisted of carbon (56.8%), nitrogen (16.4%), and hydrogen (3.6%), which was similar to the composition of pure PPy. EDX analysis indicated the presence of carbon (59.5%), nitrogen (17.4%), iron (5.2%), and chlorine (17.9%). The absence of copper supported that the linear PPy core doped with copper complex anion was etched out. Since a pyrrole has four carbons and one nitrogen, the calculated weight ratio of carbon to nitrogen is about 3.43. The ratio of carbon to nitrogen was 3.46 and 3.42 for elemental analysis and EDX analysis, respectively. Judging from these data, it is considered that the nanocapsules were composed of crosslinked PPys with iron complex anion dopant, and the residual chemicals were completely removed.

Polymerization mechanism of pyrrole

Several reports on the polymerization mechanism of pyrrole have been suggested. However, the mechanism is not clearly

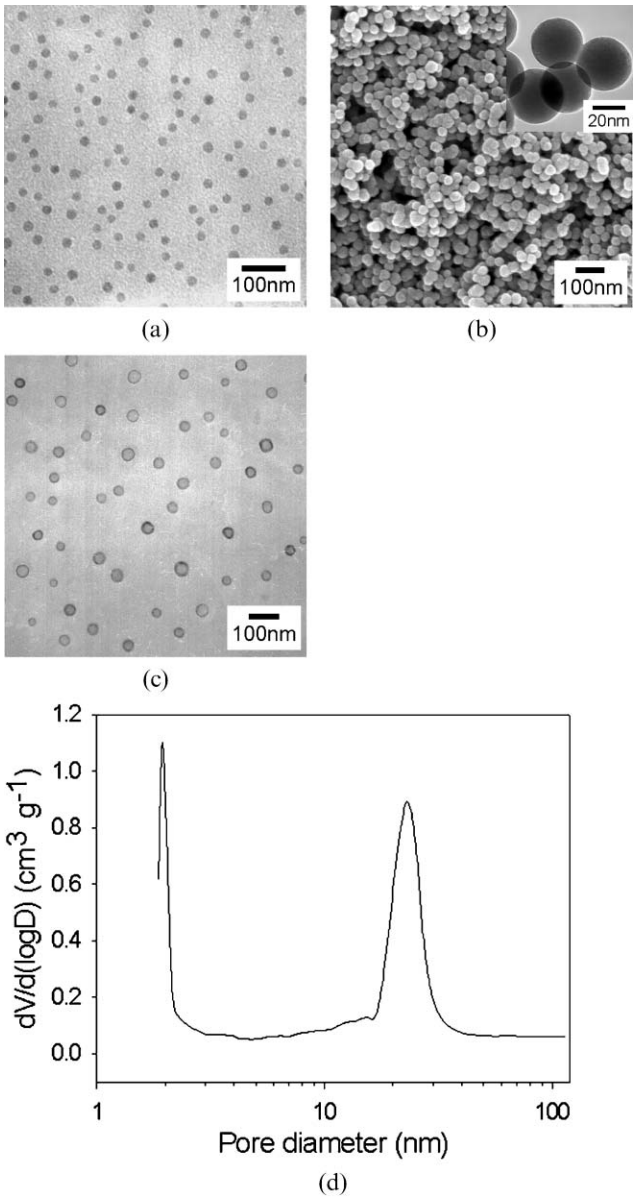

Fig. 1 TEM and SEM images of PPy nanoparticles and nanocapsules and pore size distribution of PPy nanocapsules: (a) soluble PPy nanoparticles synthesized using 0.45 M DeTAB, (b) linear PPy/crosslinked PPy core/shell nanoparticles, (c) PPy nanocapsules, and (d) the pore size distribution calculated from the nitrogen adsorption isotherm branch.

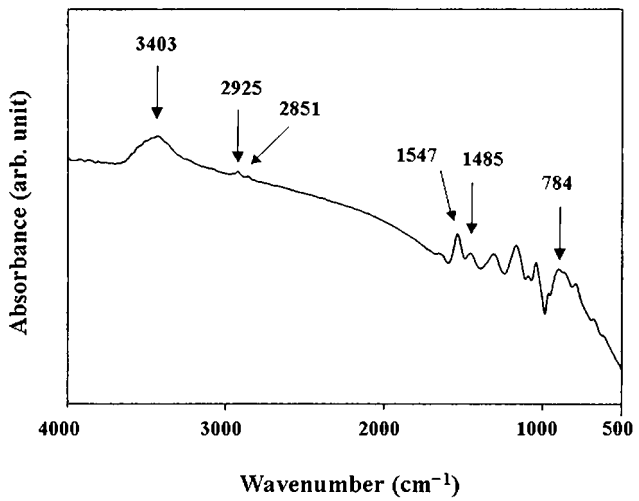

Fig. 2 FT-IR spectrum of PPy nanocapsules prepared by one-step solvent etching.

understood yet. Fig. 3 shows one of the most widely accepted mechanisms of polymerization of pyrrole.[39,40] In the initial step, radical cations ($C_4NH_5^{+\bullet}$) are produced by the oxidation of pyrrole monomer. Two of these radical cations then couple to a dimer with deprotonation, leading to a bipyrrole. After the deprotonation, the bipyrrole is reoxidized and couples with another radical cation. The process continues to form PPy chains. The termination step is known to occur owing to the nucleophilic attack of water molecules or impurities on the polymer chains.

In the pyrrole–pyrrole coupling reaction, protons in the α-position are more easily eliminated than those in the β-position. The α–α coupling reaction leads to a linear PPy, whereas the α–β coupling reaction produces a crosslinked PPy chains (Fig. 4). The α–α coupling of alternating pyrrole units gives a high degree of conjugation. Although α–α couplings are favored theoretically, the α–β couplings take place usually at the same time and break the planarity and linearity of PPy chains. In addition, over oxidation that is inevitable in aqueous polymerization process introduces a small portion of carbonyl and hydroxyl groups into the PPy chains. These nonaromatic

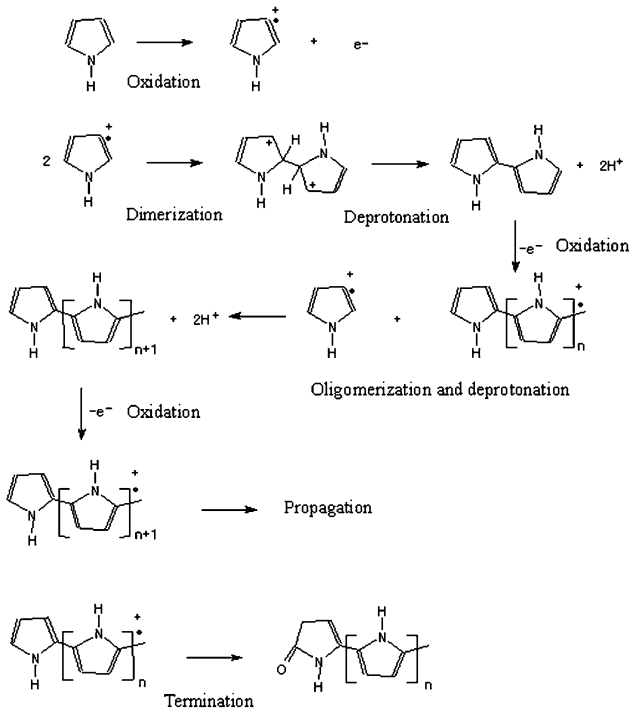

Fig. 3 Polymerization mechanism of pyrrole.

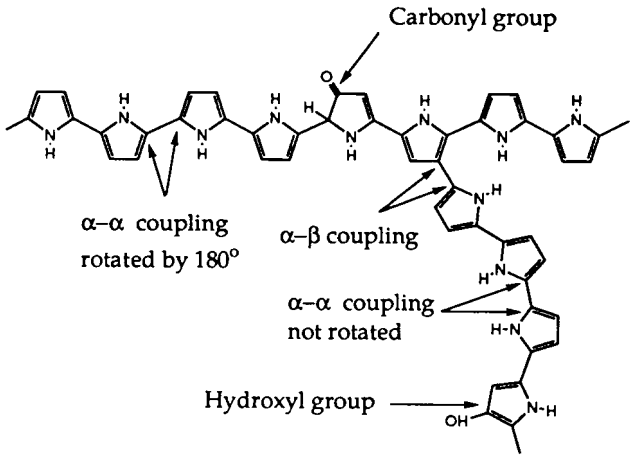

Fig. 4 Possible chemical structures in PPy chains.

bondings disturb the conjugation. All of these defects shorten the conjugation length of PPy chain and reduce the mobility of the charge carriers and finally electrical conductivity. In general, PPys synthesized either electrochemically or chemically are known to be insoluble and infusible due to the crosslinkings and the strong inter- and intramolecular interactions.[41]

Under our experimental conditions, however, highly soluble PPy was successfully synthesized by microemulsion polymerization using an oxidant with weak oxidation potential. The O/W microemulsion system prohibited the water-soluble oxidant from penetrating into the hydrophobic interior of micelles. In addition, the microemulsion system optimizes the arrangement of reactive monomer rings and increases the extent of the π-conjugation length.[42] It could be considered that the relatively weak chemical oxidation potential of the oxidant and the characteristic of microemulsion system significantly suppressed α–β coupling reaction of PPy.

The size variations of pore diameter and shell thickness of PPy nanocapsules

The pore diameter and shell thickness of PPy hollow nanospheres could be tuned by controlling the feeding amount of monomers. Fig. 5(a) represents a TEM image of PPy nanocapsules synthesized by feeding a different amount of pyrrole monomers stepwise (7.0 mmol for the core template and 32 mmol for the shell part) in 0.20 M OTAB. Copper(II) chloride and iron(III) chloride were added subsequently, based on the half of the molar quantity of pyrrole amount. The average pore size of the PPy nanocapsules was about 21 nm and the mean value of the shell thickness was approximately 10.3 nm. Fig. 5(b) shows a TEM image of PPy nanocapsules prepared by loading 6.5 mmol and 40 mmol pyrrole monomers stepwise in 0.08 M CTAB. The average diameter of PPy nanocapsules was 56 nm. The mean values of pore size and shell thickness were approximately 18 nm and 19 nm, respectively.

Fig. 6(a) and (b) show the average size changes of soluble PPy core and insoluble PPy shell thickness as a function of the feeding amount of monomers. When the surfactant (DeTAB) concentration was fixed at 0.45 M, the average diameter of soluble PPy nanoparticles was tunable from 19 to 33 nm by changing the monomer amount from 5.4 to 20.2 mmol (Fig. 6(a)). In order to evaluate the shell thickness, the crosslinked PPy shell was synthesized onto the soluble PPy cores with diameter of *ca.* 22 nm. The shell thickness also increased gradually from 5.0 to 12.5 nm with increasing the feeding amount of monomers from 14.9 to 48.5 mmol (Fig. 6(b)). These phenomena originate from the fact that the size of micelles can be enlarged to some degree with increasing the feeding amount of monomers.[32]

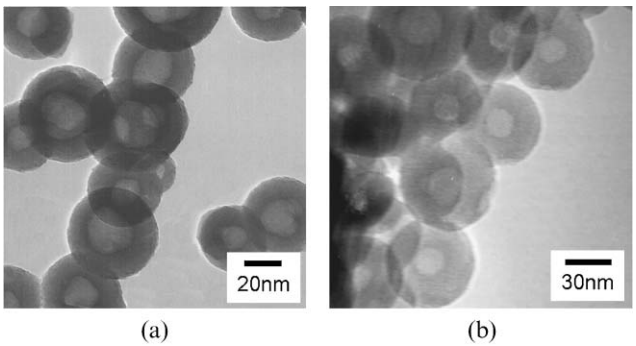

Fig. 5 TEM images of PPy hollow nanospheres synthesized by feeding a different amount of pyrrole monomers stepwise: (a) 7.0 mmol for the core template and 32 mmol for the shell part in 0.20 M OTAB, and (b) 6.5 mmol for the core part and 40 mmol in 0.08 M CTAB.

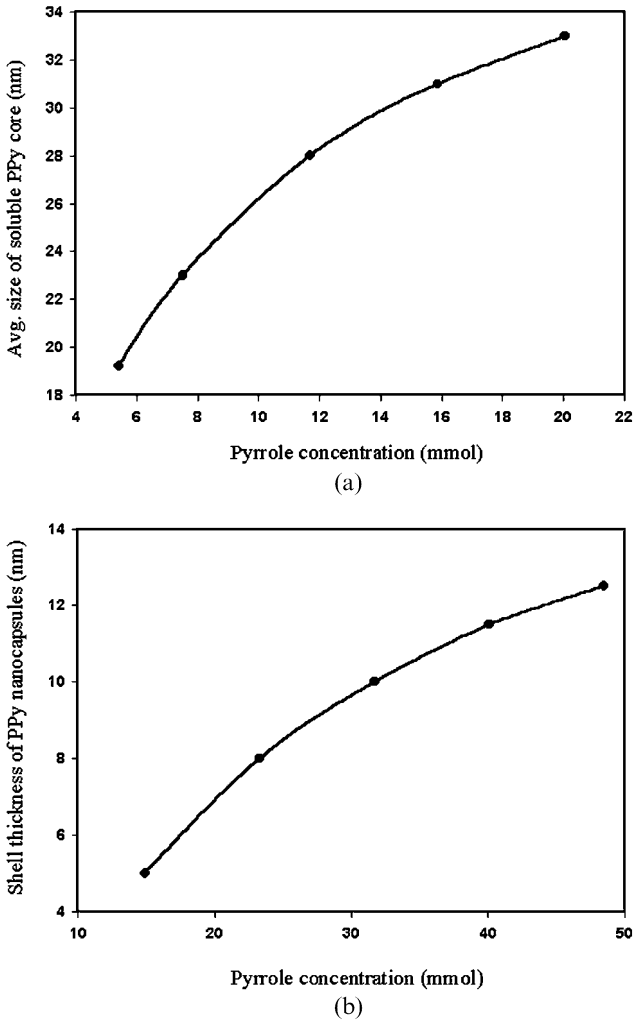

Fig. 6 (a) The diameter variation of linear PPy core with increasing monomer amount at the fixed surfactant (DeTAB) concentration of 0.45 M. (b) The shell thickness change of PPy nanocapsules as a function of the feeding amount of monomers. The soluble PPy nanoparticles with *ca.* 22 nm diameter were used as the core part.

On the other hand, the average diameter of PPy hollow nanospheres could also be tuned by adjusting the chain length and concentration of cationic surfactants. Fig. 7 represents the diameter variations of PPy nanocapsules as a function of surfactant concentration at room temperature. The average diameter of PPy nanocapsules increased with increasing the

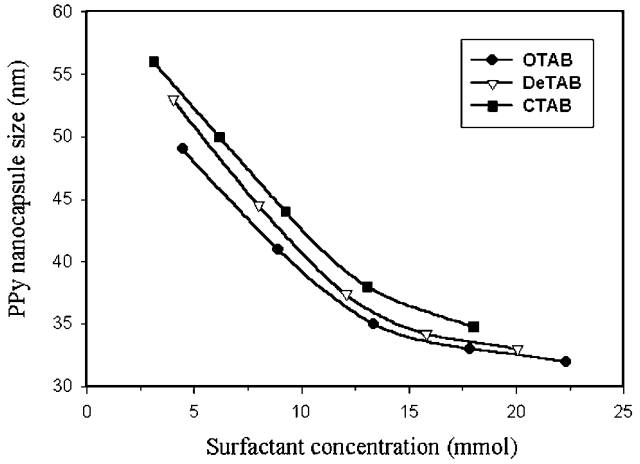

Fig. 7 The average diameter change of PPy nanocapsules as a function of surfactant concentration. The average size was determined by TEM (50 particles counted).

Table 1 Micelle aggregation number (n) and critical micelle concentration (c.m.c.) values of cationic surfactants

Surfactant	n	c.m.c./M
OTAB	20[43]	2.2×10^{-1}
DeTAB	39[44]	7.0×10^{-2}
CTAB	89[44]	9.2×10^{-4}

chain length of surfactants. This result is related with the micellar characteristics of surfactants. The enhanced flexibility of longer spacers provides more free volume inside the micelles as nanoreactors. Table 1 shows the micelle aggregation number (n) and c.m.c. of the cationic surfactants. The n is the number of surfactant molecules to form a micelle and becomes smaller with shorter hydrocarbon chain length.[43,44] This means that the number of micelles increases with shorter chain length at the same surfactant concentration, which causes the size reduction of the polymer particles synthesized at a fixed amount of monomers. The n is independent of the surfactant concentration to fairly high surfactant concentration. Therefore, the average size of polymer particles also decreases with increasing the surfactant concentration at a fixed amount of monomers because of the increment in the number of micelle nanoreactors. The c.m.c. of cationic surfactants decreases with increasing hydrocarbon chain lengths owing to the enhanced hydrophobic interactions of the spacers.

Fabrication of carbon nanocapsules

PPy hollow nanospheres could be transformed into carbon nanocapsules through the carbonization process. Fig. 8(a) exhibits a TEM image of PPy nanocapsules carbonized at 1000 °C. The average sizes of pores and shell thickness of pristine PPy nanocapsules were about 23 nm and 5 nm, respectively. However, the carbon nanocapsules showed a reduced pore size (*ca.* 21 nm) and wall thickness (*ca.* 4.5 nm). The shrinkage in the sizes results from the formation of more compact structures accompanied by denitrogenation, dehydrogenation and aromatization in the carbonization process.[45,46] EDX analysis provided the composition of the carbonized product, *i.e.* C (72.3%), N (1.2%), and Fe (3.8%). The relatively small reduction (*ca.* 9%) in diameter could be explained as follows. The carbonization process initially influences the surface structure of carbonized materials in thermodynamic respect.[47–49] Therefore, the elimination and cyclization reactions for graphitization start at the surface of the polymer nanocapsule. The graphitization proceeds by the mass-transfer flow from the inner polymer chains to the surface graphitic materials. According to our preliminary experiment, the carbonization of PPy solid nanoparticles with *ca.* 60 nm diameter produced carbon hollow nanoparticles in the similar size reduction. It is considered that these phenomena resulted in the relatively small reduction of the diameter.

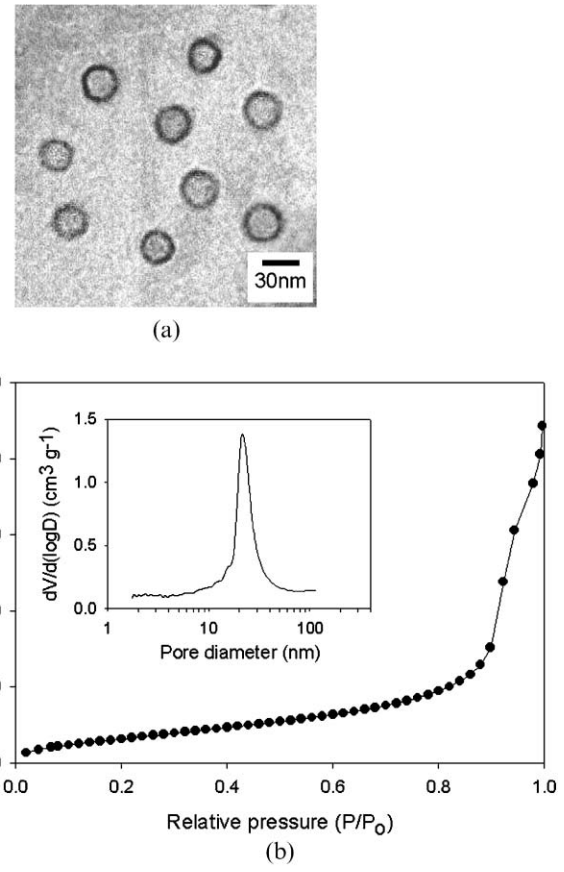

Fig. 8 (a) TEM image of carbon nanocapsules carbonized at 1000 °C. The PPy nanocapsules shown in Fig. 1(c) were carbonized. (b) Nitrogen adsorption isotherm at 350 K and pore size distribution (the inset) derived from the isotherm branch.

The pore size distribution of the carbon nanocapsules was calculated from the nitrogen adsorption isotherm branch at 350 K by the BJH method, and found to exhibit pore sizes that were fairly uniformly distributed about a center of 21 nm (Fig. 8(b)). Intriguingly, the carbon nanocapsules had no small mesopore (*ca.* 2 nm), which was observed in PPy nanocapsules. It is considered that carbonization reactions such as elimination and cyclization reactions plugs up the mesochannels in the nanocapsule wall during the carbonization process. The Brunauer–Emmett–Teller (BET) surface area of the carbon nanocapsules was *ca.* 361 $m^2\ g^{-1}$.

Fig. 9 shows a TEM image of carbon nanocapsules prepared from PPy nanocapsules synthesized by loading pyrrole monomers of 24 mmol and 22 mmol subsequently in 0.14 M CTAB. The average diameter of carbon nanocapsules had the average pore size of 32 nm and the shell thickness of *ca.* 6.5 nm, which were the values reduced by 11% compared with those of PPy nanocapsules. Fig. 10 represents the wall thickness changes as a function of the feeding amount of pyrrole monomers at the second step of the microemulsion polymerization. The other conditions were same as those in Fig. 6(b). Compared with those of PPy nanocapsules (Fig. 6(b)), 9 to 11% shrinkage in the wall thickness occurred.

XRD pattern and Raman spectrum of carbon nanocapsules carbonized at 1000 °C are illustrated in Fig. 11. The XRD pattern of carbonized hollow nanospheres confirms the presence of graphite, as the characteristic 002 and 001 Bragg reflections of graphenes are clearly displayed. The graphite 002 reflection became sharper with increasing the carbonization temperature. The 002 peak sharpening is related to the widening and thickening of the graphite layers by heat treatment.[50] The Raman spectrum of carbon nanocapsules showed two main peaks at 1580 and 1360 cm^{-1}. The band at 1580 cm^{-1} (G band) is assigned to the E_{2g} vibration of graphitic

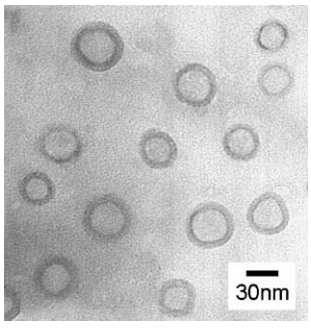

Fig. 9 TEM image of carbon nanocapsules fabricated by carbonization (1000 °C) of PPy nanocapsules that were synthesized by feeding 24 mmol and 22 mmol pyrrole stepwise in 0.14 M CTAB.

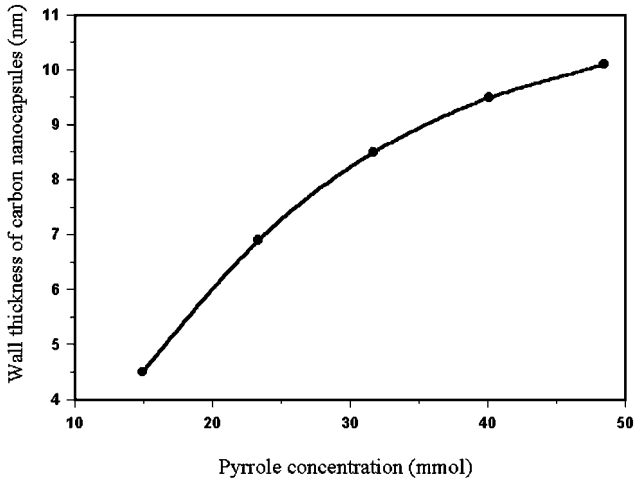

Fig. 10 Wall thickness variations as a function of the loading amount of pyrrole monomers at the second step of microemulsion polymerization. The other experimental conditions were same as in Fig. 6(b).

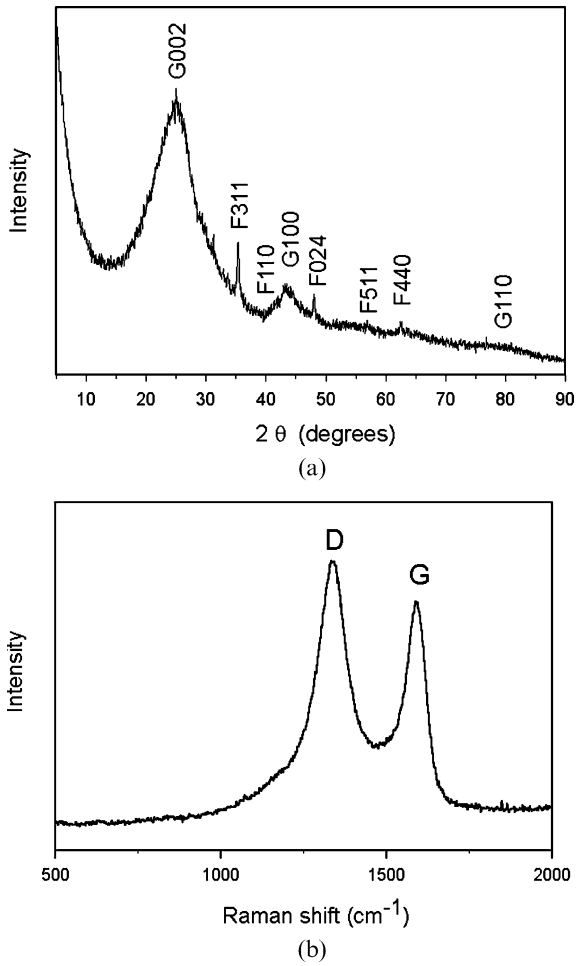

Fig. 11 (a) XRD pattern (graphite, G; γ-Fe_2O_3, F) and (b) Raman spectrum of carbon nanocapsules carbonized at 1000 °C. G and D bands on the Raman spectrum denote sp^2 and sp^3 electronic configurations, respectively.

carbon with an sp^2 electronic configuration.[51] On the other hand, the peak at 1360 cm^{-1} (D band) is attributable to the A_{1g} mode of diamond-like carbon with an sp^3 configuration.[51] The relative intensity (I_D/I_G) of carbon nanocapsules carbonized at 1000 °C was 1.19. This intensity ratio indicates a semicrystalline carbon structure containing some lattice edges or plane defects within the analyzed carbon nanocapsules.[52] When the carbonization temperature increased up to 1300 °C, the Raman spectra of the carbon nanocapsules showed an increased intensity and a decreased half width at half maximum (HWHM) of the G band, and also a decreased intensity and decreased HWHM of the D band [(I_D/I_G) = 0.68]. The decreased intensity value of I_D/I_G originated from the reduced fraction of defects within graphite-like domains. This means that structural development from a semicrystalline to a highly crystalline carbon material occurs with increasing the carbonization temperature.

The sintering effect, in which an aggregate of small particles spontaneously shrinks into a uniformly dense body when the intrinsic forces of surface tension deform the particles into space-filling shapes, as well as the fusion of the nanocapsules could produce a big carbon aggregate during the carbonization process. After the carbonization, some portion (*ca.* 10–20%) of the product had an ill-defined morphology. However, the majority of the product had a capsule-like structure, as shown by Fig. 8(a) and 9.

The HRTEM images revealed the generation of graphene layers in the wall of carbon nanocapsules. Fig. 12(a) represents a HRTEM image of carbon nanocapsule carbonized at 1000 °C. The region marked as "G" displays ordered crystalline graphene layers, whereas the area denoted as "D" exhibits an imperfect or disordered carbon region. The result is in good agreement with those of XRD and Raman spectroscopy analyses in that the carbon nanocapsule consists of the semicrystalline graphitic carbon. The degree of graphitization could be enhanced by increasing the carbonization temperature. Fig. 12(b) shows the enhanced crystallinity of the carbon nanocapsule wall at an elevated carbonization temperature (1300 °C). The degree of graphitization of the nanocapsule wall was locally different. This is considered to originate from the particle size distribution and the particle location difference in a carbonization boat in a tubular furnace. However, it was obvious that the overall degree of graphitization of nanocapsule wall was enhanced by increasing the carbonization temperature from 1000 °C to 1300 °C.

The transition metals, iron complex dopants in this experiment are known to promote the graphitization during the carbonization process.[53,54] In our experiment, the control experiment using ammonium persulfate as the comparative oxidant confirmed that the doped iron complex facilitates the graphitization of PPy nanoparticles.[32] In addition, the microemulsion system increases the extent of the π-conjugation length and optimizes the arrangement of the molecular chains.[42] The size of polymer latex synthesized by microemulsion polymerization is much smaller than that synthesized by other synthetic methods. These effects probably bring about easier cyclization and mass-transfer flow during carbonization, in our experimental conditions. It is considered that the catalytic effect of transition metal dopant and the facilitated

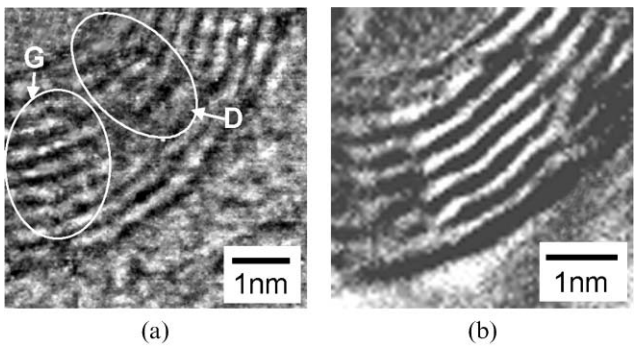

Fig. 12 HRTEM images of the wall structure of carbon nanocapsule carbonized at different carbonization temperatures: (a) 1000 °C and (b) 1300 °C. The region marked as G displays crystalline graphene layers, whereas the area denoted as D exhibits an imperfect or disordered carbon.

mass-transfer flow in carbonization reactions, which were induced by the microemulsion characteristic of polymer nanoparticle precursor, could promote the formation of graphitic species at a relatively low carbonization temperature. In addition, the degree of graphitization was higher at the outer part of the wall. This supports that the graphitization proceeds by the mass-transfer flow from inner shell polymer chains to the outer graphitic materials.

Encapsulation of a photochromic dye into polymer and carbon nanocapsules

The polymer and carbon nanocapsules were employed as a host container for the encapsulation of pyrene, a photochromic dye material. Fig. 13(a) exhibits the CLSM image of pyrene-embedded PPy nanocapsules (*ca.* 56 nm diameter) dispersed in water. Green emissions of pyrene molecules were observed in the form of solid spheres at the whole *Z*-axis sections. This means that pyrene molecules were introduced into the inner cavity of polymer capsules owing to the hydrophobic interactions. Pyrene molecule has a circular plate shape (9.8 Å × 6.3 Å).[55] The mesochannels (*ca.* 2 nm) in the polymer capsule wall could act as a passage for the introduction of pyrene molecules into the pores. The size of emission spot was slightly larger than the average pore size of PPy capsules. It is considered that some portion of pyrene molecules can be adsorbed on the outer surface of the polymer capsule.

When the CLSM observation was conducted in benzene instead of water medium, the pyrene emission was no longer concentrated in the PPy capsule, but displayed from the entire benzene medium. This is because hydrophobic pyrene molecules tend to locate at the hydrophobic interior of the polymer capsule in water medium, but the encapsulated pyrene is released from the polymer capsule in the hydrophobic benzene medium. This result reveals the potential of the polymer capsule as a nano-sized container for storage and release of organic guest molecules in a different environment.

Fig. 13(b) displays a CLSM image in the water-phase experiment of carbon nanocapsule (*ca.* 52 nm diameter). The fluorescence of pyrene showed a doughnut shape emission when focusing the *Z*-axis section on the center of carbon capsule. This means that the concentration of pyrene molecules was higher at the surface of the carbon nanocapsule than that at the inner cavity. The relatively bulky pyrene molecule could not be introduced into the inner cavity of carbon nanocapsule because of the absence of mesochannels in the capsule wall. Instead, pyrene molecules were adsorbed on the outer hydrophobic surface of carbon capsule in water medium. The doughnut-like emission of pyrene molecules disappeared in benzene medium, where the pyrene molecules were dissolved into the hydrophobic medium.

Although the carbon nanocapsules could not be utilized as a host container for bulky pyrene molecules, they possess large specific area and might possibly entrap Li ions into the graphitic layers, which provides a feasibility of the application as an anodic material in lithium-ion batteries.

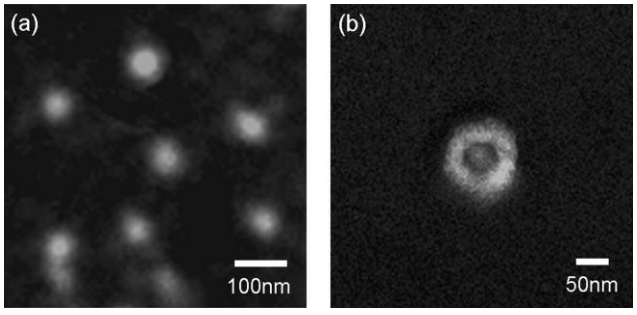

Fig. 13 CLSM fluorescence images of (a) PPy nanocapsule and (b) carbon nanocapsule. Pyrene molecules were loaded in aqueous phase.

Conclusions

Linear PPy/crosslinked PPy core/shell nanospheres were synthesized stepwise by microemulsion polymerization using two oxidants (copper(II) chloride and iron(III) chloride) with different chemical oxidation potentials. One-step alcohol etching of soluble PPy core and cationic surfactants produced crosslinked PPy nanocapsules. The pore size and shell thickness were controllable by changing the feeding amount of monomers in each synthetic step. The average diameter of PPy nanocapsules decreased with increasing the concentration of surfactant and decreasing the spacer length of surfactant. In addition, the PPy hollow nanospheres could be transformed into carbon nanocapsules through the carbonization process. The graphitization of carbon capsule wall was facilitated with increasing the carbonization temperature, and the degree of graphitization was higher at the outer part of the wall. The carbonization reactions such as elimination and cyclization reactions for graphitization start at the surface of the polymer nanocapsule. The graphitization is considered to proceed by the mass-transfer flow from inner shell polymer chains to the outer graphitic materials. PPy nanocapsules had two mesopores, that is, the large inner cavity and the small mesochannel that was produced during the solvent etching process. The PPy nanocapsules showed the selective encapsulation and release property (controllable permeability) of pyrene molecules into the inner cavity in a different environment. In aqueous medium, carbon nanocapsules mainly exhibited a doughnut shape emission from pyrene molecules adsorbed onto their outer surface. This arose from the lack of channels to allow the penetration of pyrene molecules into the cavity. This conceptually new and simple methodology has allowed the facile fabrication of polymer and carbon nanocapsules with tunable pore and shell sizes, and might be expanded for the fabrication of other polymeric capsules, embracing the concept of solubility difference of the same polymer.

Acknowledgements

This work has been financially supported by the Brain Korea 21 program of the Korean Ministry of Education and the Hyperstructured Organic Materials Research Center supported by Korea Science and Engineering Foundation.

References

1 R. Langer, *Science*, 1990, **249**, 1527.
2 E. Donath, G. B. Sukhorukov, F. Caruso, S. A. Davis and H. Möhwald, *Angew. Chem., Int. Ed. Engl.*, 1998, **37**, 2202.
3 F. Caruso, R. A. Caruso and H. Möhwald, *Chem. Mater.*, 1999, **11**, 3309.
4 N. Gaponik, I. L. Radtchenko, M. R. Gerstenberger, Y. A. Fedutik, G. B. Sukhorukov and A. L. Rogach, *Nano Lett.*, 2003, **3**, 369.
5 D. G. Shchukin, G. B. Sukhorukov and H. Möhwald, *Angew. Chem., Int. Ed. Engl.*, 2003, **42**, 4472.
6 C. A. Morris, M. L. Anderson, R. M. Stroud, C. I. Merzbacher and D. R. Rolison, *Science*, 1999, **284**, 622.
7 H. Feilchenfeld, G. Chumanov and T. M. Cotton, *J. Phys. Chem.*, 1996, **100**, 4937.
8 J. Jang and J. H. Oh, *Adv. Mater.*, 2003, **15**, 977.
9 J. Jang and B. Lim, *Angew. Chem., Int. Ed. Engl.*, 2003, **42**, 5600.
10 E. Wilson, *Chem. Eng. News*, 1999, **77**(5), 32.
11 F. Caruso, D. Trau, H. Möhwald and R. Renneberg, *Langmuir*, 2000, **16**, 1485.
12 I. Gill and A. Ballesteros, *J. Am. Chem. Soc.*, 1998, **120**, 8587.
13 S. M. Marinakos, J. P. Novak, L. C. Brousseau III, A. B. House, E. M. Edeki, J. C. Feldhaus and D. L. Feldheim, *J. Am. Chem. Soc.*, 1999, **121**, 8518.
14 J. Jang and H. Ha, *Chem. Mater.*, 2003, **15**, 2109.

15 F. Caruso, R. A. Caruso and H. Möhwald, *Science*, 1998, **282**, 1111.
16 F. Caruso, *Adv. Mater.*, 2001, **13**, 11.
17 C. J. McDonald, K. J. Bouck, A. B. Chaput and C. J. Stevens, *Macromolecules*, 2000, **33**, 1593.
18 J. Jang and K. Lee, *Chem. Commun.*, 2002, 1098.
19 W. J. Macknight, E. A. Ponomarenko and D. A. Tirrell, *Acc. Chem. Res.*, 1998, **31**, 781.
20 A. Harada and K. Kataoka, *Science*, 1999, **283**, 65.
21 Q. Zhang, E. E. Remsen and K. L. Wooley, *J. Am. Chem. Soc.*, 2000, **122**, 3642.
22 H. Huang, E. E. Remsen, T. Kowalewski and K. L. Wooley, *J. Am. Chem. Soc.*, 1999, **121**, 3805.
23 D. H. W. Hubert, M. Jung and A. L. German, *Adv. Mater.*, 2000, **12**, 1291.
24 M. Zhao, L. Sun and R. M. Crooks, *J. Am. Chem. Soc.*, 1998, **120**, 4877.
25 M. S. Wendland and S. C. Zimmerman, *J. Am. Chem. Soc.*, 1999, **121**, 1389.
26 X. Liu, M. Jiang, S. Yang, M. Chen, D. Chen, C. Yang and K. Wu, *Angew. Chem., Int. Ed. Engl.*, 2002, **41**, 2950.
27 M. Wang, G. Zhang, D. Chen, M. Jiang and S. Liu, *Macromolecules*, 2001, **34**, 7172.
28 J. Jang, X. L. Li and J. H. Oh, *Chem. Commun.*, 2004, 794.
29 V. K. Aswal and P. S. Goyal, *Chem. Phys. Lett.*, 2002, **364**, 44.
30 G. D'Errico, O. Ortona, L. Paduano and V. Vitagliano, *J. Colloid Interface Sci.*, 2001, **239**, 264.
31 D. Yan, J. L. Jordan, V. Burapatana and G. K. Jennings, *Langmuir*, 2003, **19**, 3357.
32 J. Jang, J. H. Oh and G. D. Stucky, *Angew. Chem., Int. Ed. Engl.*, 2002, **41**, 4016.
33 J. Jang and K. Lee, *Chem. Commun.*, 2002, 1098.
34 J. Jang and J. H. Oh, *Chem. Commun.*, 2002, 2200.
35 J. Jang and J. H. Oh, *Adv. Mater.*, 2003, **15**, 977.
36 G. Odian, *Principles of Polymerization*, Wiley, New York, 1991, Ch. 4.
37 H. G. Barth, *Modern Particle Size Analysis*, Wiley, New York, 1984, p. 111.
38 C. Kvarnström and A. Ivaska, in *Organic Conductive Molecules and Polymers*, ed. H. S. Nalwa, Wiley-VCH, Weinheim, 1997, ch. 9.
39 A. J. Heeger, in *Handbook of Conducting Polymers*, ed. T. A. Skotheim, Marcel Dekker, New York, 1986, p. 4.
40 G. H. Gorman and R. H. Grubbs, in *Conjugated Polymers*, ed. J. L. Bredas and R. Silbey, Kluwer Academic Publishers, Dordrecht, 1991, p. 3.
41 R. Qian, in *Conjugated Polymers and Related Materials*, ed. W. R. Salaneck, I. Lundström and B. Ranby, Oxford University Press, London, 1993, p. 161.
42 F. Yan, G. Xue and M. Zhou, *J. Appl. Polym. Sci.*, 2000, **77**, 135.
43 M. Drifford, L. Belloni and M. Dubois, *J. Colloid Interface Sci.*, 1987, **118**, 50.
44 P. Lianos and R. Zana, *J. Colloid Interface Sci.*, 1981, **84**, 100.
45 J. Jang and J. H. Oh, *Chem. Commun.*, 2004, 882.
46 E. Ando, S. Onodera, M. Iino and O. Ito, *Carbon*, 2001, **39**, 101.
47 A. Braun, M. Bärtsch, B. Schnyder, R. Kötz, O. Haas and A. Wokaun, *Carbon*, 2002, **40**, 375.
48 D. Ugarte, *Carbon*, 1995, **33**, 989.
49 Y. Saito, *Carbon*, 1995, **33**, 979.
50 G. T. Fey and Y. C. Kao, *Mater. Chem. Phys.*, 2002, **73**, 37.
51 A. W. P. Fung, A. M. Rao, K. Kuriyama, M. S. Dresselhaus, G. Dresselhaus, M. Endo and N. Shindo, *J. Mater. Res.*, 1993, **8**, 489.
52 M. S. Dresselhaus, P. C. Eklund, G. Dresselhaus and M. J. Pelletier, *Analytical Application of Raman Spectroscopy*, Blackwell Science, Oxford, 1999, ch. 9.
53 H. Oka, M. Inagaki, Y. Kaburagi and Y. Hishiyama, *Solid State Ionics*, 1999, **121**, 157.
54 A. M. Herring, J. T. McKinnon, B. D. McCloskey, J. Filley, K. W. Gneshin, R. A. Pavelka, H.-J. Kleebe and D. J. Aldrich, *J. Am. Chem. Soc.*, 2003, **125**, 9916.
55 J.-K. Lee, W.-K. Koh, W.-S. Chae and Y.-R. Kim, *Chem. Commun.*, 2002, 138.